Chinese Journal of Chemical Engineering 83 (2025) 217–228

Contents lists available at ScienceDirect

Chinese Journal of Chemical Engineering

journal homepage: www.elsevier.com/locate/CJChE

Full Length Article

Efficient hydrogen evolution from Amberlyst-15 mediated hydrolysis of ammonia borane under mild conditions

Yilun Dong [1, 2, 3], Kang Xue [1, 2, 3, 4, *], Zexing He [1, 2, 3], Chongjun Li [1, 2, 3], Ruijie Gao [1, 2, 3, 4], Zhenfeng Huang [1, 2, 3, 4], Chengxiang Shi [1, 2, 3, 4], Xiangwen Zhang [1, 2, 3, 4], Lun Pan [1, 2, 3, 4], Jijun Zou [1, 2, 3, 4, *]

[1] *Key Laboratory for Green Chemical Technology of the Ministry of Education, Institute of Molecular Plus, School of Chemical Engineering and Technology, Tianjin University, Tianjin 300072, China*
[2] *National Industry-Education Platform for Energy Storage, Tianjin University, Tianjin 300072, China*
[3] *Collaborative Innovative Center of Chemical Science and Engineering (Tianjin), Tianjin 300072, China*
[4] *Haihe Laboratory of Sustainable Chemical Transformations, Tianjin 300192, China*

ARTICLE INFO

Article history:
Received 2 November 2024
Received in revised form
21 January 2025
Accepted 19 February 2025
Available online 30 April 2025

Keywords:
Ammonia borane
Hydrolysis
Hydrogen production
Amberlyst-15
Kinetics

ABSTRACT

The efficient and cost-effective implementation of ammonia borane (AB) hydrolysis dehydrogenation for hydrogen storage is crucial. This study investigated the role of solid acid Amberlyst-15 (A-15) for hydrogen evolution from AB hydrolysis. Notably, AB hydrogen evolution rate can reach 194.15 ml·min^{-1} at 30 °C, with a low apparent activation energy of 8.20 kJ·mol^{-1}. After five cycles of reuse, the reaction involving A-15 could keep a conversion rate of about 93%. The AB hydrolysis follows quasi first-order kinetics with respect to the AB concentration and quasi zero-order kinetics with respect to the A-15 mass. According to the characterization results of XRD, ATR-FTIR, and *in-situ* MS, the boric acid was the dominant hydrolyzate, while water as a hydrogen donor in this reaction. Furthermore, based on the reasoning that hydrogen bonds between A-15 and AB (aq) promotes the diffusion of AB, release of H_2 and the cleavage of O—H bond of H_2O, a possible mechanism was proposed.

1. Introduction

Currently, hydrogen storage remains one of the key issues limiting the widespread application of the hydrogen energy [1–4]. Among chemical hydrogen storage methods, ammonia borane (NH_3BH_3, AB), which has the advantages of high stability and easy transportation [4,5], owns a mass hydrogen storage density of up to 19.6% that far exceeds the mass hydrogen storage density target of 4.5% proposed by the US Department of Energy for in vehicle hydrogen storage systems [6]. Meanwhile, AB has the characteristics of being stable at room temperature and non-toxic. The main ways for releasing hydrogen from AB include thermolysis, alcoholysis, and hydrolysis (Eq. (1), typical reaction equation of AB hydrolysis) [7]. Solid AB thermolysis is not suitable for hydrogen evolution due to the generation of many by-products and high reaction temperature [8]. The latter two methods can both achieve hydrogen evolution under mild conditions, especially for the hydrolysis of AB to produce hydrogen, water as a solvent is cheaper than alcohol solvents [9,10]. For the hydrolysis reaction of AB is relatively slow, metal catalysts are generally used to accelerate this process. Researchers have successively developed a series of catalysts, including metal catalysts, metal compound catalysts, and photo assisted hydrolysis catalyst [11–14], among which noble metal catalysts have better catalytic effects [5,15]. Chandra and Xu [13] tested the dehydrogenation of AB by noble metal catalysts and found that the activation energy of Ru/γ-Al_2O_3, Rh/γ-Al_2O_3 and Pt/γ-Al_2O_3 are 23, 21, and 21 kJ·mol^{-1}, and the reactions were completed within 3, 1.3, and 0.75 min, but the high price of these noble metal limited their further application. For non-noble metal catalysts, transition metals Co, Ni, Cu and their alloys [16–18] have received more attention, but their reaction rates and turnover frequency (TOF) are still not comparable to noble metal catalysts.

$$NH_3BH_3 + 3H_2O \rightarrow NH_4^+ + B(OH)_4^- + 3H_2 \quad (1)$$

Recently, liquid acids have been shown to participate in the hydrolysis of AB to produce hydrogen [19,20], which greatly

* Corresponding authors.
E-mail addresses: xuekang@tju.edu.cn (K. Xue), jj_zou@tju.edu.cn (J. Zou).

https://doi.org/10.1016/j.cjche.2025.02.030

increased the rate of hydrogen release and even directly reacted with AB to release hydrogen. And some weak acids [19,21], also can react with AB, but they cannot completely release H_2 in equal amounts of AB. Moreover, it has been confirmed that solid acids such as H-type molecular sieves, Dowex, and Amberlyst can hydrolyze AB to produce hydrogen, and Amberlyst-15 can achieve dehydrogenation reaction rates comparable to noble metal catalysts [22]. In addition, Li *et al.* [19] suggest that the AB hydrolysis process involving acids is essentially similar to the process of strong acids generating weak acids (Eq. (2)), in that the acids introduce hydrogen protons, which promotes the dissociation of B—N bonds, ultimately releasing H_2 and producing boric acid.

$$H(ACS) + NH_3BH_3 + 3H_2O \rightarrow H_3BO_3 + NH_4(ACS) + 3H_2 \quad (2)$$

Furthermore, considering that solid acids can efficiently achieve kinds of reactions, as well as the advantages of avoiding container corrosion compared to liquid acids and being able to separate from the system after reaction [23–25], solid acids are selected as templates to explore the performance of acid in hydrogen evolution from AB hydrolysis and its reaction mechanism. Among solid acids, a strong acidic ion-exchange resin composed of divinylbenzene (DVB) and styrene, with sulfonic acid groups as active sites after polymerization and sulfonation, is inexpensive, highly reactive and easy to regenerate and reuse after reaction. Among this type of resin, A-15 is widely used in acid catalytic processes due to its superior physical properties [26,27]. In addition, A-15 has been shown to participate in the hydrolysis hydrogen evolution reaction of AB [22], and own fast reaction rate. Though Derya Oncel *et al.* [28] had used A-15 as a Ru catalyst support and applied it to the hydrolysis reaction of AB, the direct reaction of A-15 as a solid acid with AB has not been investigated, so this process needs to be further s explored in more detail.

Therefore, in order to obtain an efficient and inexpensive AB hydrolysis hydrogen production system, the performance superiority of AB hydrolysis dehydrogenation with A-15 participation was proved (the hydrogen evolution rate of 194.59 $ml \cdot min^{-1}$ at 30 °C, the E_a of 8.20 $kJ \cdot mol^{-1}$). Meanwhile, its well reusability has also been experimentally proven. Furthermore, a kinetic study of the AB hydrolysis dehydrogenation process with A-15 was completed to clarify the reaction order. The hydrogen donor (water), main hydrolysate (boric acid) and reaction formula were determined using isotope substitution experiments, XRD, ATR-FTIR, and *in-situ* MS. The presence of hydrogen bonds between O in the sulfonic acid group of A-15 and AB (aq) were confirmed through ATR-FTIR, and a possible hydrolysis mechanism based on the promotion of AB diffusion and O—H bond cleavage of H_2O was proposed. The research results are believed to support an economical technical approach of hydrogen evolution form AB hydrolysis and provide fundamental insights into the mechanism study of the acid-involved AB hydrolysis reaction.

2. Experimental

2.1. Materials

Ammonium borane complex (NH_3BH_3, 97%), cation exchange resin Amberlyst-15 (H) (particle size 0.045 mm), sodium hydroxide (NaOH, AR), potassium chloride (KCl, AR), methyl orange (96%), boric acid (H_3BO_3, AR), metaboric acid (HBO_2, AR) and deuterium chloride (DCl, D% = 99.999%) were purchased from Shanghai Meryer Chemical Technology Co., Ltd. Deionized water was self-made in the laboratory (conductivity>18.25 $M\Omega \cdot cm^{-1}$). Deuterated water (D_2O, D% = 99.999%) was purchased from Cambridge Isotope Laboratories, Inc. Hydrochloric acid (HCl, AR) and sulfuric acid (H_2SO_4, AR) were purchased from Fengchuan Chemical Reagent Technology Co. Sodium citrate ($C_6H_5Na_3O_7$, 98%) was purchased from Aladdin Reagent Co., Ltd. Sodium hypochlorite (NaClO, [Cl] = 5.0% (mass)) was purchased from Macklin Biochemical Technology Co. Sodium nitroferricyanide dihydrate ($C_5H_4FeN_6Na_2O_3$, 99%) and salicylic acid ($C_7H_6O_3$, 99.5%) was provided by Tianjin Heowns Biochemical Technology Co., Ltd.

2.2. Characterization techniques

X-ray powder diffraction (XRD) was performed using a D/Max-2500 (RIKEN) with a graphite monochrome filter and a Cu Target K_α (λ = 154 nm), the working voltage was 40 kV, and the scanning speed was 10 $(^\circ) \cdot min^{-1}$. Fourier transform infrared spectroscopy (FT-IR) were acquired with a Bruker INVENIO S spectrometer using a diamond single reflection attenuated total reflectance (ATR) device. Sample spectra was obtained at 15 kHz scanner velocity with RT-DlaTGS as detector in the wavenumber range from 4000 to 400 cm^{-1}. SHIMADZU UV-2600 was used for UV-vis. Mass spectrometry (MS, Linglu Instruments, QAS 100, ion source: EI, 70 eV, detector: SEM) was used as *in-situ* technique for qualitative analysis to determine the deuterium labeled gas products. Reactants were added into the open reaction tank, where produced gas molecules diffused onto the waterproof breathable membrane, then drawn into the mass spectrometry detector by a vacuum pump for *in-situ* product analysis. Since the reaction tank was open, only qualitative data could be provided. Asap2460 automatic adsorption instrument of micromeritics was used for N_2 adsorption/desorption. When in use, the sample to be tested was degassed by vacuum pretreatment at 120 °C, and then transferred to the adsorption instrument. The test was carried out in liquid nitrogen (−196 °C). The pore volume of the sample can be calculated from the amount of N_2 adsorption/desorption under different pressures. The Brunauer-Emmett-Teller (BET) method was used to calculate the specific surface area of the sample. The adsorption branch data and Barrett-Joyner-Halenda (BJH) method were used to calculate the mesopore distribution of the sample.

2.3. Experimental procedure

2.3.1. Hydrogen evolution device

The schematic diagram of hydrolysis activity testing system for AB is shown in Fig. 1, which consists of a hydrogen production unit and a gas collection unit. The hydrogen production unit is a three-neck reactor with a jacket, with the one outlet sealed with rubber plugs serving as the injection ports. Another outlet is connected to the gas collection device through a rubber tube. And the upper opening of the reactor is sealed with a flange. The gas collection unit reflects the volume of gas by the mass of discharged water. The mass variation of discharged water with time was automatically recorded by an electronic balance (TD 50001A, Tianjin Tianmahengji Instrument Co., Ltd.) connected to a computer. Finally, the gas product volume is calculated by dividing the recorded mass of discharged water by the water density at the ambient temperature.

2.3.2. Pretreatment of A-15

Activation of A-15: To maintain consistent activity, the ion-exchange resin A-15 needs to be activated before test. The A-15 was placed into a beaker, soaked and washed with deionized water, and then the A-15 particles were immersed in a 2 $mol \cdot L^{-1}$ HCl (aq) for 24 h. The acid solution was then poured out and A-15 was rinsed with deionized water until the washing solution pH was 7. Finally, the activated A-15 particles were dried in an oven at 60 °C for 24 h.

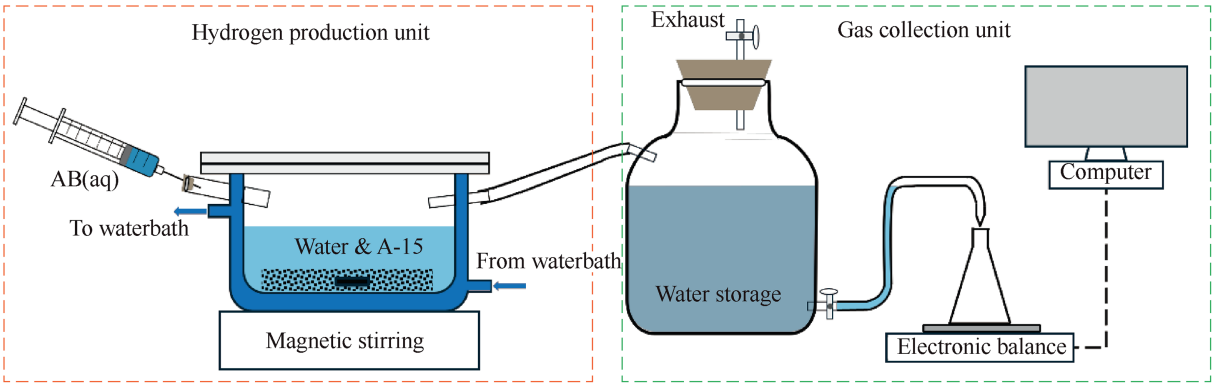

Fig. 1. Hydrolytic hydrogen evolution device.

Deuteration of A-15: A certain amount of A-15 was immersed in a prepared excess of 1 mol·L^{-1} NaOH deuteroxide solution for 24 h, then the solution was poured out, and A-15 was rinsed with deuteroxide (D_2O). Then, an excess of 1 mol·L^{-1} DCl deuteroxide solution was add to soak A-15 for 24 h. Subsequently, A-15 was rinsed with D_2O until the pH of the washing solution was 7. Finally, the deuterated A-15 particles were dried in an oven at 60 °C for 24 h.

2.3.3. Acid content determination

The acid content of A-15 is determined by titration. 0.60 g A-15 was added into a conical flask and then 30 ml 0.1 mol·L^{-1} NaOH (aq) was added and immersed for 24 h under sealed conditions. After that, two drops of 1% (mass) methyl orange solution were added as a chromogenic reagent. Subsequently, NaOH (aq) containing A-15 was titrated with 0.1 mol·L^{-1} of HCl (aq) using a 50 ml acidic burette, until the solution turned light orange red and did not fade for 30 s. The total amount of acid on A-15, representing the amount of proton hydrogen on the A-15 sulfonic acid group, was obtained by subtracting the HCl (aq) amount reflected by titration terminal volume from the NaOH mole of 30 ml 0.1 mol·L^{-1} NaOH (aq).

2.3.4. Activity testing

When conducting activity testing, 0.60 g A-15 and 10 ml deionized water were added to the reactor and stirred at the reaction temperature for 10 min. The reaction was triggered by rapidly injecting 5 ml AB solution (0.3 mol·L^{-1}, if concentration is not specified) into reactor through a syringe. At the same time, the reaction time and hydrogen production were synchronously recorded by an electronic balance. The reaction temperature was controlled by a jacket (30 °C, if not specified). The reaction stirring rate was controlled at 1200 r·min^{-1} through magnetic stirring. The overall hydrogen evolution rate (k) was calculated based on Eq. (3).

$$k = \Delta V/\Delta t \tag{3}$$

where ΔV is the straight part of the hydrogen evolution curve (the part of conversion 0% to 80%), Δt is corresponding reaction time.

2.3.5. Ammonia content detection

The ammonia was quantitatively determined by the indophenol blue method [29]. When testing, taked 2 ml of the test solution, added 2 ml of chromogenic reagent, 1 ml NaClO (aq), and 0.2 ml reducing agent (specific components is in Supplementary Material), and stored in the dark for 2 h. Afterwards, the absorbance in the range of 550–750 nm was measured by UV-vis to obtain the characteristic peak absorbance around 655 nm, and the ammonia content value was calculated based on the external standard curve (Fig. S1, Supplementary Material).

3. Results and Discussion

3.1. Hydrogen evolution reaction

Firstly, the effect of stirring speed on the hydrolysis reaction was investigated to eliminate the influence of external mass transfer resistance on the reaction as much as possible. The gas production of the reaction was measured sequentially at 400, 800, 1000, 1200, and 1400 r·min^{-1}. As shown in Fig. S2, with the increase of stirring speed, the reaction rate increases from 149.53 ml·min^{-1} at 400 r·min^{-1} to 194.15 ml·min^{-1} at 1200 r·min^{-1}. This can be attributed to the enhanced stirring process accelerating the external diffusion process and improving the reaction rate. And in the reaction, because of the little solution, using a stirring speed of 1400 r·min^{-1} would splash the solution and decrease the reaction rate. Therefore, to prevent the reaction solution splashing into the exhaust port and better control the experimental variables, 1200 r·min^{-1} was chosen as the stirring speed for subsequent experiments. Supplementary reactions have also been conducted to ensure consistency in performance testing (Fig. S3).

Subsequently, the effect of A-15 on the reaction was tested at 30 °C and 1200 r·min^{-1}. The test results are shown in Fig. 2(a), the reaction rate of A-15 reached 194.15 ml·min^{-1} with only 0.60 g A-15. However, for having poor mechanical strength, A-15 appeared as powders after the reaction. Considering that the active site of A-15 is the proton acid on the sulfonic acid group, to further investigate the hydrolysis process of AB facilitated by A-15, the acid content of A-15 (the proton hydrogen content on the sulfonic acid group) was quantified. As shown in Table S1, the average proton acid content of approximately 2.8 mmol of H^+ per 0.60 g A-15 (4.67 mmol·g^{-1}) was determined through three titrations. Therefore, the reactivity of A-15 was compared with that of liquid acid in the same acid content. As illustrated in Fig. 2(a), the reactions using 2.8 mmol HCl (aq) and 1.4 mmol H_2SO_4 (aq), matching the acid content of 0.60 g of A-15, could totally complete, with hydrogen evolution rates of 178.80 and 196.46 ml·min^{-1}. The difference in diffusion rates between liquid acids and solid acids is particularly intriguing. In theory, the mass transfer resistance in liquids is significantly lower than in solids. However, in practice, for resins like A-15, they do not behave purely as solids in water; instead, they exist in a gel network and the mass transfer capability of swollen resins is quite respectable [25,30]. Meanwhile, the lower mechanical strength of A-15 allows it to be gradually stirred into powders during the reaction, which could also reduce external diffusion resistance. So, the rate difference between H_2SO_4 (aq) and A-15 is not significant. It is noteworthy that the hydrogen evolution rate of AB with HCl (aq) is slightly lower than that of A-15 and H_2SO_4 (aq) at the same acid content suggesting that there are other

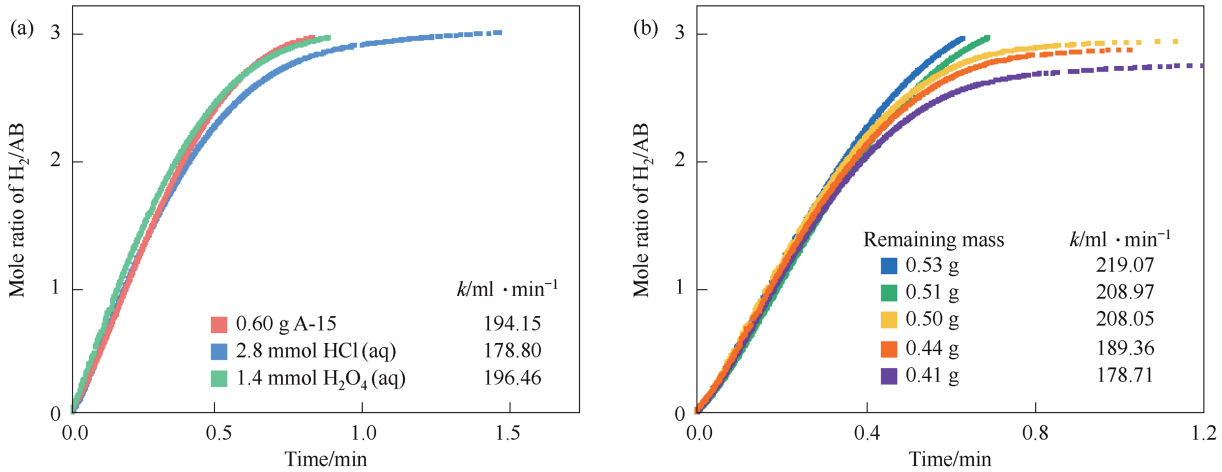

Fig. 2. (a) Hydrogen evolution performance of A-15, HCl (aq) and H_2SO_4 (aq) for AB hydrolysis at the same acid content. (b) The recycling test of A-15 for AB hydrolysis.

Table 1
Typical acid involved AB hydrolysis performance.

Acid	Complete reaction time/min	Reaction ability[①]/mol·g^{-1}	Mole ratio (H_2/AB)	Reference
A-15	0.83	4.67	3.00	This work
HCl (aq)	1.49	0.0328	3.00	This work
H_2SO_4(aq)	0.88	0.0220	3.00	This work
Pure acetic acid	5.5	/	1.22	[19]
Acetic acid (aq)	10	/	2.55	[19]
Citric acid (aq)	<30	0.0052	3.00	[20]

① Reaction ability represents the mole of AB that can be completely reacted by 1 g acid (without considering the solvent mass).

interactions between A-15 and AB participating in the reaction to accelerate the reaction, which made A-15 faster than HCl (aq). As shown in Table 1, the performance of several reported acids that can achieve AB hydrolysis are compared. A-15 has a faster reaction rate and can also achieve complete reaction. Especially, as a solid acid, A-15 could convert more AB per unit mass. Anyway, combining the advantages of avoiding container corrosion and being able to separate from the system after reaction compared to liquid acids, A-15 has greater application potential of AB hydrolysis.

As a cation exchange resin, A-15 can be reused through reactivation, and tests were conducted to evaluate its reusability at 30 °C and 1200 r·min^{-1}. After reaction, A-15 was collected by centrifugation, washed with water, and then reactivated for subsequent reactions. As shown in Fig. 2(b), the first two batches of recovered A-15 could fully react, whose reaction rates are 219.07 and 208.97 ml·min^{-1}. Being stirred and crushed into powders after the first reaction resulted in lower mass transfer resistance of the A-15. Therefore, the recovered reaction rate is faster than the initial reaction using the 0.45 mm particles of A-15. After five cycles of reuse, the reaction involving A-15 can still release approximately 105.46 ml of H_2, achieving a conversion rate of about 93% and a reaction rate of 178.71 ml·min^{-1}. Furthermore, the normalized hydrogen evolution rate (the ratio of hydrogen evolution rate to A-15 mass) of reused A-15 was evaluated (Table S2). In the five recovery reactions, the normalized hydrogen evolution rate does not change significantly, indicating that the mass of A-15 could not extremely affect the reaction rate and the hydrolysis of AB is of the quasi zero-order reaction in A-15. The decrease in reaction rate and conversion could be attributed to the inevitable mass loss and structure destruction of A-15 during the recovery, washing, and reactivation processes, as well as the precipitation of boric acid and subsequent partial overlay of active sites on the A-15 surface after multiple reactions [31,32]. Although the activity of A-15 decreased after multiple uses, it could still maintain a conversion of 93%. If the mass loss during the regeneration process could be reduced, the decrease of conversion rate and reaction rate is expected to be further minimized.

As shown in Table 2, the pore diameter and pore volume of activated A-15 are slightly decreased, due to the structural damage caused by acid treatment and drying, which indicated that the activation process caused damage to the pore structure of A-15. After the reaction, regardless of stirring, the specific surface area and pore volume of A-15 decreased, which is related to some products (boric acid or ammonia salts) may adhere to the pores after the reaction [31,32], reducing the surface area. Meanwhile, the specific surface area and pore volume decrease from 25.963 m^2·g^{-1} and 0.2464 cm^3·g^{-1} to 21.168 m^2·g^{-1} and 0.2119 cm^3·g^{-1} after the reaction with stirring as compared to without stirring. This is mainly due to the poor mechanical strength of A-15, most of which was stirred by magnetic particles during the reaction, thus causing further damage to the A-15 structure. But the pore diameter of A-15 does not change significantly before and after the reaction, which most remain around 39 nm. The SEM, TEM and actual images are also taken (Figs. S11 and S12). The morphology of A-15 changes from spherical particles to powder during the activation and reaction processes. However, the microscopic pore size of A-15 does not change much, and the difference before reaction and after reaction without stirring is not obvious, which is consistent with the BET results.

Subsequently, to analyze the main liquid phase product of the reaction, ATR-FTIR was used to characterize the solid powders obtained by drying the supernatant of the hydrolysis reaction residues. As shown in Fig. 3(a), the peaks at approximately 3139 cm^{-1} and 1409 cm^{-1} respectively correspond to the stretching and bending vibration of O—H, and 1192 cm^{-1} corresponds to the

Table 2
Textural parameters of A-15.

A-15 Sample	S_{BET}/m^2·g^{-1}	V_{total}/cm^3·g^{-1}	D_{pore}/nm
Before activated	27.75	0.3292	48.47
Before reaction	27.83	0.2636	39.86
After reaction (without stirring)	25.96	0.2464	39.81
After reaction (with stirring)	21.16	0.2199	39.83

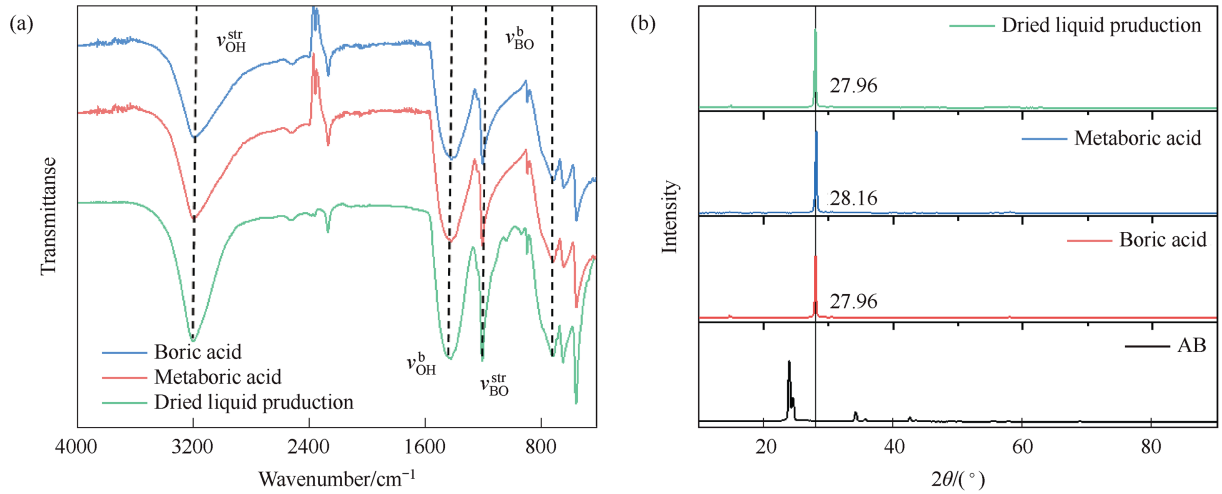

Fig. 3. (a) ATR-FTIR spectra of dried liquid products. (b) XRD patterns of dried liquid products.

stretching vibration of B—O, while 709 cm^{-1} for the bending vibration of B—O [33]. The difference between sample and boric acid or metaboric acid around 2300 cm^{-1} may be caused by the masking of signals by residual A-15 in the sample. However, ATR-FTIR cannot determine whether the product is boric acid or metaboric acid.

In order to exactly verify the main liquid phase products, XRD was applied. Though the sample inevitably contained a small amount of A-15, considering that the polymer synthesized from divinylbenzene (DVB) and styrene has no typical crystal structure (Fig. S4), it would not affect the characterization results. Through XRD characterization of the solid powder, as shown in Fig. 3(b), it's clear that there is a very strong peak at $2\theta = 27.96°$, which is the characteristic peak of boric acid [12]. And the characteristic peak position is basically consistent with the boric acid standard sample. In addition, according to the XRD results of the AB raw material powders used, all AB was completely consumed and there was no residue after reaction. Meanwhile, by correlating the ATR-FTIR results with the XRD results, it can be concluded that the dominate hydrolyzate of hydrolysis is boric acid. Besides, the ^{11}B-NMR results (Fig. S5) also prove that the liquid products have a same peak as boric acid [20], which proves this conclusion.

3.2. Kinetics of AB hydrolysis reaction

To further evaluate the performance of A-15, the kinetics of AB hydrolysis dehydrogenation were tested. Firstly, the effect of different reaction temperatures on the hydrolysis rate of AB was investigated (0.60 g A-15 and 15 ml 0.1 mol·L^{-1} AB (aq)), as shown in Fig. 4(a). As the reaction temperature increased from 30 to 60 °C, the time for complete release of 113.4 ml of H_2 continues to decrease, and the hydrogen evolution rate (k) increases from 194.15 to 261.72 ml·min^{-1}. The Arrhenius plot can be obtained by correlating the logarithmic reaction rate (ln(k)) with 1/T and the slope of the plot show that the apparent activation energy (E_a) of the hydrolysis of AB with A-15 participation is 8.20 kJ·mol^{-1}. Compared to some typical metal catalysts [13,34–43], the E_a of this reaction is lower. This lower E_a means that the reaction rate of the AB hydrolysis involving A-15 is less affected by the reaction temperature and more likely to occur, so this system can respond quickly to produce H_2 at room temperature, which proved the superior performance of A-15. And considering that the price of A-15 is much lower than that of Pt catalyst [44], A-15 owns more advantages in the application of AB hydrolysis dehydrogenation.

Subsequently, the effects of the usage of A-15 and the concentration of AB solution on the hydrogen evolution from AB hydrolysis were tested. Fig. 4(c) illustrates experiments conducted with varying masses of A-15 from 0.10 g to 1.20 g reacted with 15 ml 0.1 mol·L^{-1} AB (aq), it is found that when the mass of A-15 is higher than 0.30 g, AB (aq) is able to react completely, and the reaction rate does not be significantly accelerated with the increase of usage. In Fig. 4(d), the ln(k) and ln(A-15) (the logarithmic A-15 masses ranging from 0.40 g to 1.2 g) are correlated to estimate the reaction order, which is 0.07504, indicating that the hydrolysis of AB is of the quasi zero-order reaction in A-15. This also indicates that the reaction rate is limited by the proton hydrogen on the sulfonic acid groups on the surface of A-15, rather than the quantity of A-15 itself. Besides, the normalized hydrogen evolution rate of different mass A-15 has the same changing trend as reusability tests (Table S3).

Next, the influence of varying concentrations of AB on the reaction rate was tested. Fig. 4(e) shows the reaction rates using 0.60 g A-15 in the hydrolysis reaction of 15 ml of AB (aq) with different concentrations, the reaction rate continues to increase with the increase of AB (aq) concentration. Up to 0.20 mol·L^{-1}, the addition of A-15 cannot completely release H_2, thus the reaction rate maintaining at 284.46 ml·min^{-1} without greater increase. The ln$k$ is plotted and fitted against ln(AB) (logarithmic concentrations of AB ranging from 0.10 to 0.18 mol·L^{-1}), yielding a slope of 0.750. This indicates that the hydrolysis of AB follows quasi first-order kinetics with respect to the concentration of AB (Fig. 4(f)). The reactions in higher AB (aq) concentrations (0.33 and 1 mol·L^{-1} with 0.60 g A-15) have also been tested (Fig. S6), and the results show that A-15 can react with higher concentrations of AB (aq), but cannot completely release hydrogen. Besides, based on the maximum release H_2 of 212.11 ml, it is estimated that 0.60 g A-15 will fully react 2.81 mmol AB.

Overall, A-15 enhances the AB hydrolysis hydrogen evolution reaction with low activation energy and a fast reaction rate. Moreover, A-15 is cost-effective and minimizes container corrosion compared to liquid acids, and it can be easily separated and reused [26,27]. Therefore, compared with commonly used noble metal catalysts, A-15 has an exciting potential for application in the dehydrogenation process of AB hydrolysis as a solid acid.

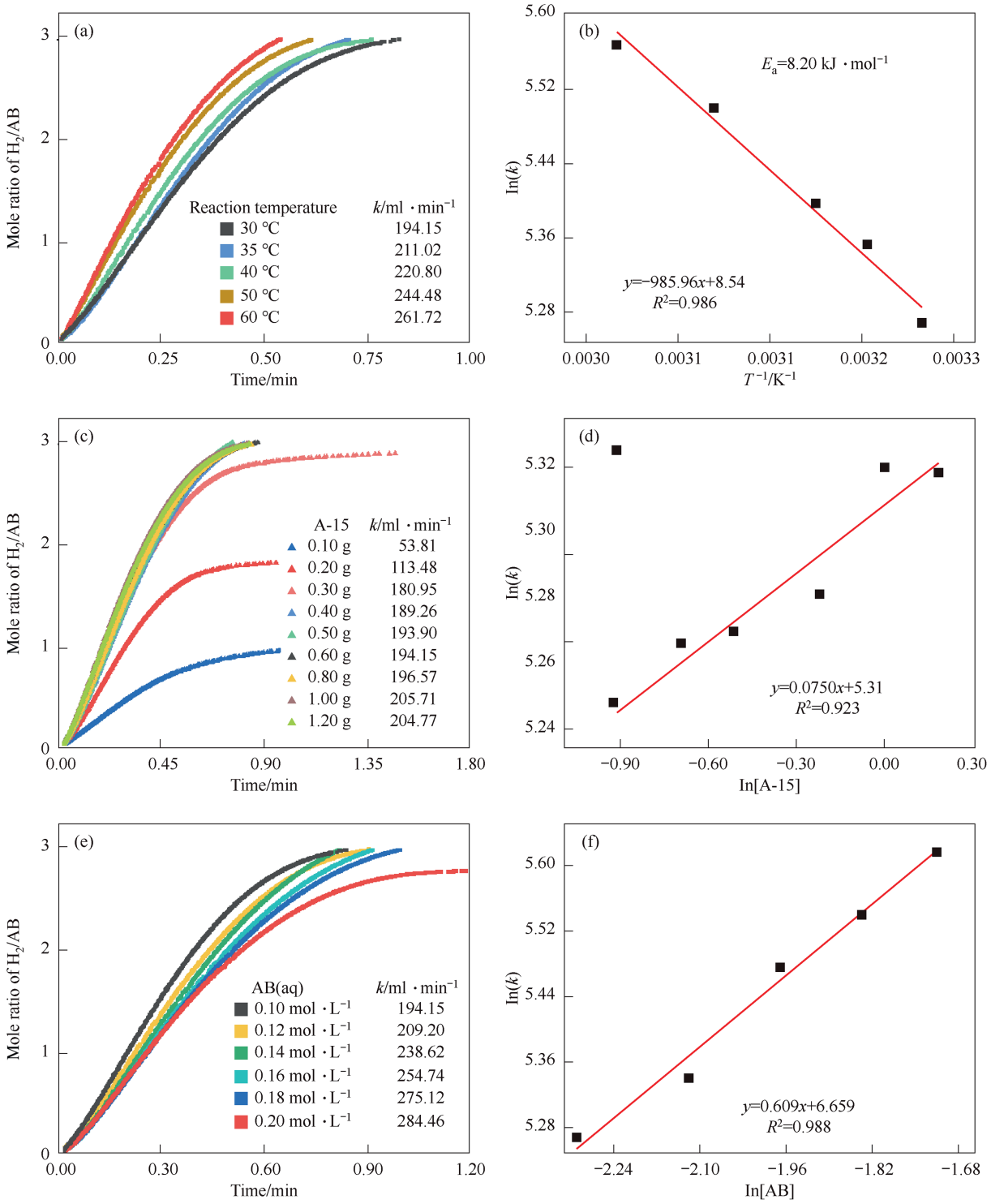

Fig. 4. (a) Hydrogen evolution of AB hydrolysis at different temperatures. (b) ln$k$ *versus* 1/T for AB hydrolysis. (c) Hydrogen evolution of AB hydrolysis with different masses of lnA-15. (d) Logarithmic plot of H_2 evolution rate *versus* ln [A-15] and corresponding fitting line. (e) Hydrogen evolution of AB hydrolysis with different concentrations of AB. (f) Logarithmic plot of H_2 evolution rate *versus* ln[AB] and corresponding fitting line.

3.3. AB hydrolysis mechanism

To explore the effect of acid content, the HCl (aq) was chosen for offering the more accurate acid content. As depicted in Fig. 5(a), different concentrations of HCl (aq) reacted with 15 ml 0.1 mol·L^{-1} AB (aq). When the amount of HCl reaches 1.5 mmol, AB (aq) can be fully reacted. The amount of HCl is correlated with the actual hydrogen evolution (V_0), showing a strong linear relationship as illustrated in Fig. 5(b). This indicates that acid content impacts on hydrogen evolution. In theory, the hydrolysis of AB to produce

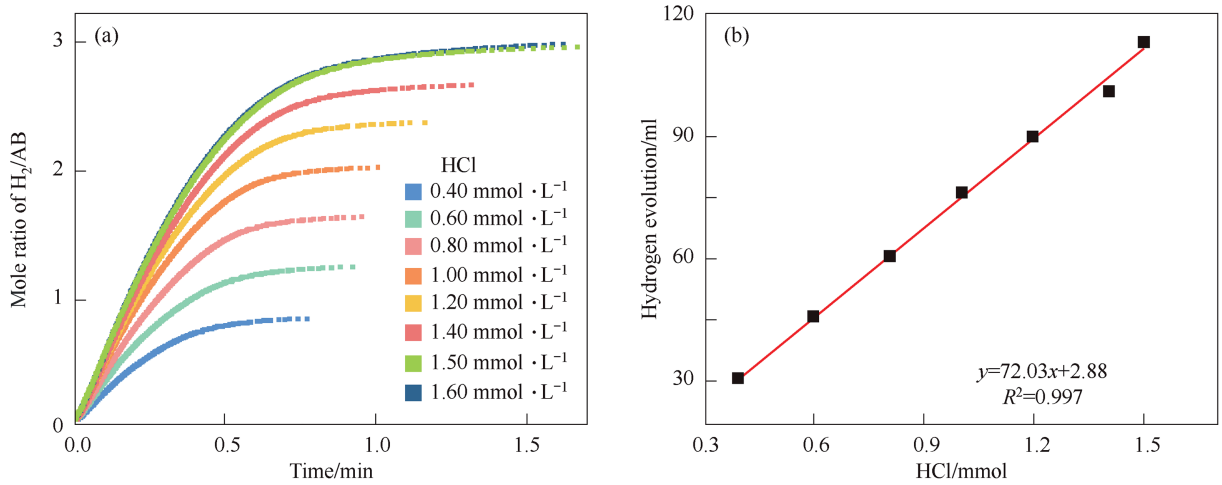

Fig. 5. (a) Hydrogen evolution of AB hydrolysis with different moles of HCl. (b) Corresponding fitting line of hydrogen evolution and mole of HCl.

hydrogen is essentially a process of proton hydrogen and the hydrogen charged negatively on B—H binding to release H_2. The H_2 generated by this process is called the direct hydrogen evolution (V_1). It is found that the values of V_0: V_1 from 0.40 mmol to 1.4 mmol are basically 3:1 (Table S4), which indicates that proton hydrogen can react with equimolar amounts of AB in aqueous solution and release three times hydrogen. So, in this process, water shall provide H twice as much as acid. Otherwise, only 4.5 mmol HCl could fully react with 1.5 mmol AB. In addition, based on the inference that proton hydrogen can react equimolar amounts of AB, and considering the acid amount of A-15, each gram of A-15 can react with 4.67 mmol AB and release 354.4 ml H_2, which similar to the results calculated through kinetics studies (0.60 g A-15 could fully react 2.81 mmol AB). However, in order to further confirm the role of water and proton hydrogen from A-15 in this reaction, further experiments are necessary.

To further verify the hydrogen donor in the reaction, isotope substitution experiments was performed to detect the gases generated during the reaction by *in-situ* MS (Fig. S7). Firstly, 10 mg of A-15 was added to 1 ml of D_2O, and then 10 μl 0.1 mol·L^{-1} AB (dissolved in D_2O) was added dropwise. As shown in Fig. 6(a), after adding AB solution, signals with similar molecular weights of 2 and 3 (2_amu and 3_amu) are detected, which indicates the generation of H_2 and deuterated hydrogen (DH) during the reaction. Since only D_2O can provide deuterium (D) in this reaction, the emergence of DH proved that in the AB hydrolysis reaction with A-15, H_2O participated in the reaction and provided H. Meanwhile, a low intensity signal with 4_amu (D_2) is also detected, which may be due to ion exchange of AB during the reaction in D_2O, resulting in possible partial substitution of H on B—H by D. Additionally, there is no significant signals of 17_amu (NH_3). This can be attributed to the low concentration of AB solution in the reaction and the temperature being controlled by the water-cooled jacket at 30 °C, so no NH_3 was released [33].

Afterwards, to further verify, 10 mg of deuterated A-15 was added to 1 ml of H_2O, and then 10 μl 0.1 mol·L^{-1} AB (aq) was added dropwise (Fig. 6(b)). After adding deuterated A-15, significant H_2 and DH signal are observed, this proves that the proton hydrogen in A-15 take part in this reaction. The signal intensity of H_2 is much greater than that of the DH, which once again prove that water is an important hydrogen donor in the hydrolysis of AB with acids participation. Meanwhile, there are no significant signals of NH_3 or D_2, which also indicate that the appearance of D_2 is not related to the proton hydrogen on A-15. Besides, the difference in signal

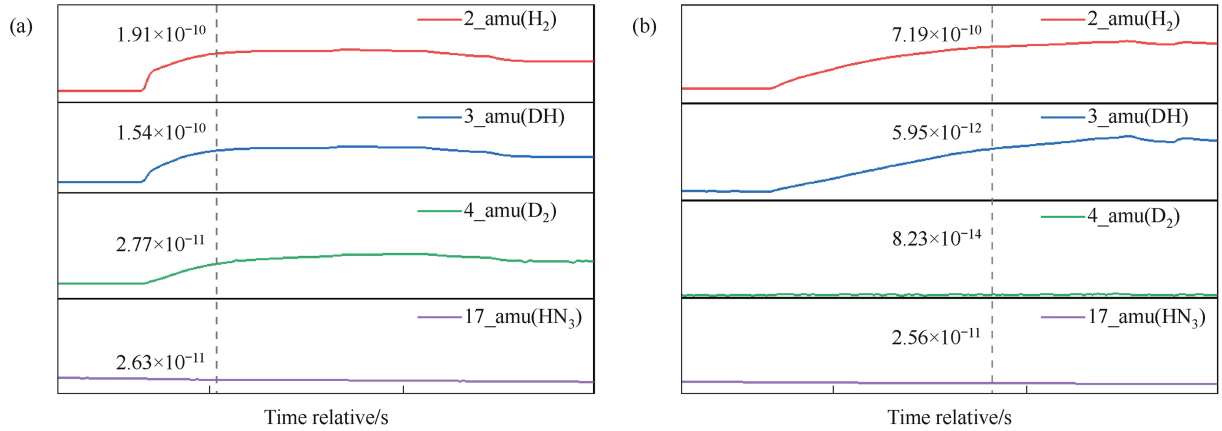

Fig. 6. *In-situ* MS patterns of (a) dropping 10 μl 0.1 mol·L^{-1} AB (in D_2O) to 1 ml D_2O with 10 mg A-15 and (b) dropping 10 μl 0.1 mol·L^{-1} AB (aq) to 1 ml H_2O with 10 mg deuterated A-15.

intensity of 3_amu between these two figures can be attributed to the primary hydrogen donor is not A-15 and the incomplete deuteriation of A-15.

Considering that the process of AB producing H_2 in the proton solvent is similar to the elimination reaction between negatively charged hydrogen and proton hydrogen, AB would provide negatively charged hydrogen, the rest of positively charged hydrogen needs to be provided by proton solvent (such as water, methanol) [15]. However, with the participant of A-15, positively charged hydrogen is not only provided by water, but also the proton acid from A-15. Furthermore, based on the XRD, ATR-FTIR, ^{11}B-NMR and *in-situ* MS results, the reaction process of AB involving A-15 can be represented by the following reaction formula (Eq. (4)):

$$NH_3BH_3 + H^+ + 3H_2O \rightarrow NH_4^+ + B(OH)_3 + 3H_2 \quad (4)$$

Furthermore, to clarify the destination of ammonia, UV-vis was used to detect the content of NH_4^+ in the solution. Reaction started with 0.60 g A-15 at 30 °C and 1200 r·min^{-1}. During the reaction, connect the outlet rubber tube of the reactor to a beaker filled with 100 ml H_2O to collect any possible ammonia gas. The test results (Table S5, Fig. 7) show that the NH_4^+ content in the solution after the reaction was 4.67×10^{-3} mol·L^{-1}, which was much lower than the theoretical maximum concentration of 0.1 mol·L^{-1}. Meanwhile, consistent with the *In-situ* MS results, the NH_4^+ content in the gas-washing solution can be almost negligible. Considering that A-15 is a cation exchange resin, a significant portion of the NH_4^+ produced by the reaction may be ion-exchanged onto A-15. So, rinsed the reacted A-15 three times with 50 ml deionized water, collected and detected the NH_4^+ content in this 150 ml solution, whose result was 1.10×10^{-4} mol·L^{-1}, a very low content, indicating that the residual solution on A-15 after the reaction has been washed away. Then separated and added the washed A-15, to 30 ml of KCl (aq), sonicated for 5 min for cation exchange, and then measured the NH_4^+ content. After ion exchange, the NH_4^+ in the solution increases significantly, approaching half of the theoretical maximum NH_4^+ content (4.36×10^{-2} mol·L^{-1}), suggesting that a significant portion of the ions are exchanged onto A-15. And part of the remaining NH_4^+ is dissolved in the solution, whose content is relatively small, so the relevant ammonium salts are not detected in infrared and XRD. The other NH_4^+ may form salts with boric acid and attach to A-15, and thus cannot be fully exchanged into solution [31,32].

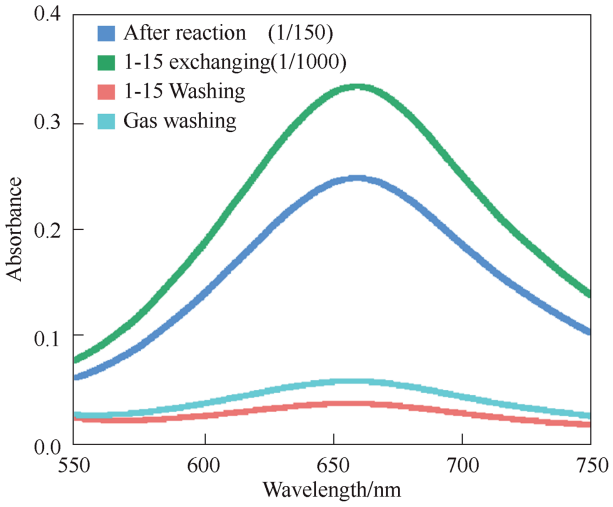

Fig. 7. The UV-vis results of NH_4^+ content in four different solutions (after reaction, A-15 exchanging, A15 washing and gas washing). 1/150 and 1/1000 is volume dilution ratio.

Due to the limitations of the N—H···H—B network between AB molecules and the hydrogen bonds network formed with water [45], the AB hydrolysis rate in aqueous solution is generally slow. It can be considered that the proton hydrogen plays a role similar to activated reaction [19]. But for A-15, there should be additional interactions between A-15 and AB participating in the reaction to accelerate it. It was found that hydrogen bond (HB) and dihydrogen bond (DHB) could reduce the reaction energy barrier of AB hydrolysis and accelerate the reaction [44,46,47]. Considering that O in the sulfonic acid group of A-15 could form hydrogen bonds with H, it is inferred that it can enhance the reaction.

For this purpose, ATR-FTIR was used to investigate the hydrogen bonds in the reacted A-15 and AB (aq). The ATR-FTIR spectra were shown in Fig. 8 and Fig. S8. As shown in Fig. 8(a)–(b), compared to the A-15 sample, the symmetric vibrational peaks (about 1004 cm^{-1} and about 1028 cm^{-1}) of S═O in the mixture shift towards higher wave numbers with the addition of AB (aq). And with the increase of A-15 content, the degree of shifting become slightly greater. It's believed that this shift indicates the formation of hydrogen bonds between O (in S═O) and H [48]. Additionally, the symmetric vibrational peaks intensity also significantly decreases, which may be attributed to the decrease in the relative content of A-15 after the addition of AB (aq). The intensity of the asymmetric vibration peak of S═O (about 1126 cm^{-1}) also decreases, while the wider peak become narrower due to the influence of the adjacent B—H deformation bend peak of AB (about 1176 cm^{-1}). Meanwhile, the signal intensity of the hydroxyl stretching vibration peak (about 3600–3000 cm^{-1}) decreases with increasing A-15 content, indicating that the hydroxyl H in water may also form HB with the O in S═O on A-15.

To investigate the influence of HB formed by water, hydrogen bonds in mixtures of varying A-15 concentrations and water were further investigated. As illustrated in Fig. 8(c)–(d), the symmetric vibrational peak of S═O in the mixture of water and A-15 also shift towards higher wave numbers, but the shifting is smaller than that in the mixture with added AB (aq) (Fig. S9), indicating the presence of HB between A-15 and AB. For asymmetric vibration peaks, they are observed to split in water. This can be due to HB limiting the symmetric stretching vibration of S═O, making it more asymmetrical. This also suggests that the changes in symmetric vibration peaks of S═O in A-15 and AB mixtures are not only caused by the proximity of B—H deformation bend peaks of AB. Meanwhile, the intensity of the S═O characteristic peak of A-15 in water is also higher, which may be attributed to the less infrared signal masking by pure water compared to AB (aq). In addition, at the hydroxyl stretching vibration peak, the intensity decreases more in the mixture with added AB (aq) than in the mixture with added water at the same A-15 content (Fig. S9), indicating the presence of hydrogen bonds between AB and water.

Further testing was conducted on the hydrogen bonds in a mixture containing 5 ml each of 1, 2, and 4 mol·L^{-1} AB (aq) and 0.3 g of A-15 powders (Fig. 8(e)–(f)). It is found that as the AB content increase, the S═O asymmetric vibration peak shift towards higher wave numbers, confirming the formation of HB between A-15 and AB.

In order to investigate the rate determining step of the reaction, the kinetic isotope effect experiment of AB hydrolysis over A-15 was performed. Substituted H_2O with D_2O in AB hydrolysis, the reaction rate slows down (Fig. S10). The kinetic isotope effect constant (KIE, k_{H_2O}/k_{D_2O}) is about 2.19, which means that the breaking of the O—H bond of H_2O is the rate determining step [49,50]. This also indicates that the limitation of mass transfer resistance on the reaction is not decisive.

AB producing H_2 in water is similar to the elimination reaction between negatively charged hydrogen and proton hydrogen, but

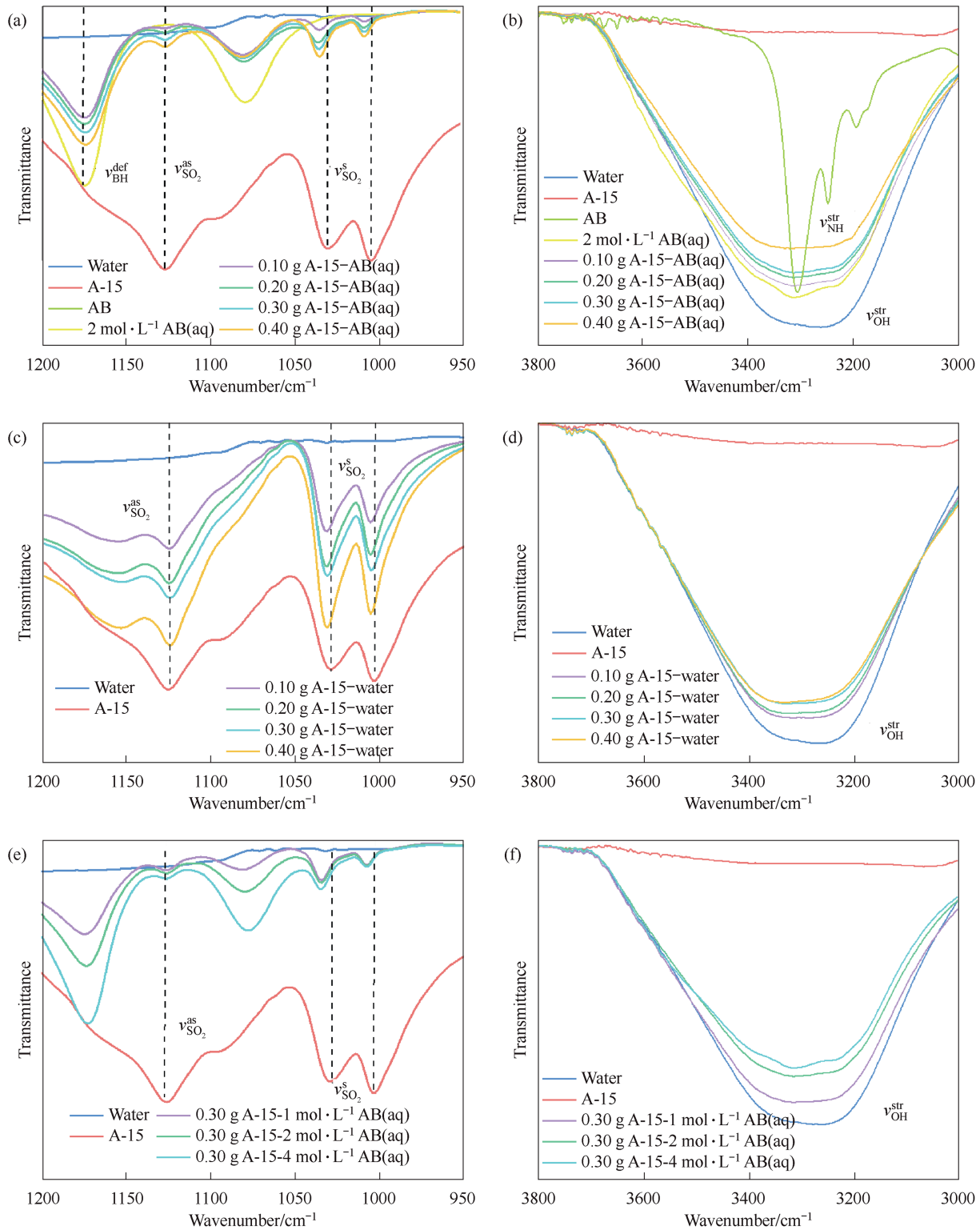

Fig. 8. ATR-FTIR spectra of (a, b) different mass A-15 with 2 mol·L^{-1} 5 ml AB (aq), (c, d) different mass A-15 with 5 ml water and (e, f) 0.30 g A-15 with different concentrations of 5 ml AB (aq).

the first step of releasing hydrogen is not the same in different systems [15]. For example, the combinations of electronegativity $H^{\delta-}$ of —BH_3 in AB with electropositivity $H^{\delta+}$ in acid is believed to be the first step of the H_2 release in the reaction of CH_3COOH and AB [19]. Meanwhile, researchers also report that H_2 could be released between negatively charged hydrogen and hydrogen protons on AB through DHB [51,52]. Similarly, it has been confirmed that HB could promote the reaction in the AB hydrolysis whose RDS is the dissociation of water [45–47]. Referring to existing experimental and characterization results, DHB and DB

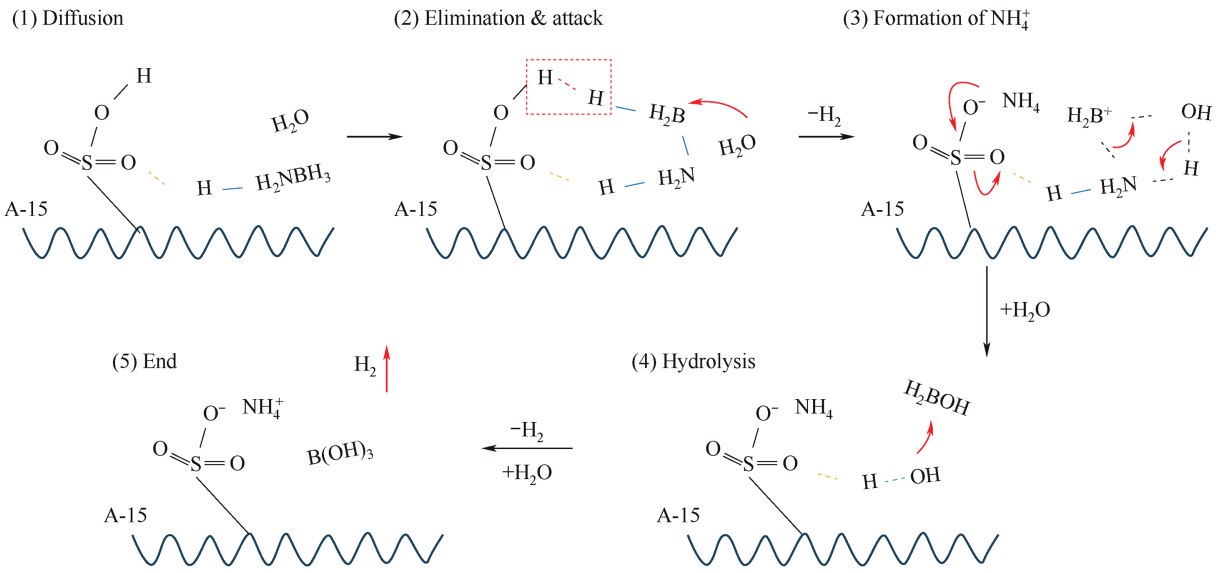

Fig. 9. Proposed mechanism for AB hydrolysis with A-15 participation.

are undoubtedly key factors in the AB hydrolysis process involving A-15.

Based on the existence and function of hydrogen bonds, it is speculated that the AB hydrolysis process with A-15 participation can be divided into several stages as shown in Fig. 9. (1) The S═O of the sulfonic acid group and the N—H in AB form hydrogen bond, promoting the diffusion of AB towards A-15 and increasing the concentration of AB near the surface of A-15 [46]. (2) The negatively charged hydrogen on —BH_3 combines with the proton hydrogen on the sulfonic acid group of A-15 to form DHB and realizes hydrogen elimination [19,51], which could effectively reduce the energy barrier for H_2 release [45,46]. The breaking of B—H bond also further exposes B atom, increasing its positive charge and reducing steric hindrance, which is conducive to water nucleophilic attack on B atom. (3) Nucleophilic attack causes the cleavage of B—N, while H of H_2O transfers to form NH_4^+. Then, it is attracted by the negative charge on the sulfonic acid group to exchange ions onto A-15, which has been confirmed by the determination of ammonia. (4) The HB between H_2O and O of sulfonic acid groups would length the H—O bond in water to reduce its strength [53,54], while the O of water attacking on B atom, the cleavage of H—O bond of water (the RDS of AB hydrolysis) [19,55] could be facilitated, which lowers the activation barrier. After H—O bond cleavage, the H transfers to the O of sulfonic acid group, subsequently eliminating the negatively charged hydrogen from the B—H bond and releasing hydrogen. Then $BH(OH)_2$ would undergo a similar process, and hydrolysis process completed. (5) The reaction concludes and ultimately forms boric acid, with ammonium ions bound to A-15. Although a tentative dehydrogenation mechanism has been assumed, further systematic research shall be needed for elucidating the effects of spatial structure [56] of A-15.

4. Conclusions

In this work, A-15 was selected to participate in the hydrogen evolution from AB hydrolysis. The hydrogen evolution rate of AB hydrolysis involving A-15 can reach 194.15 ml·min^{-1} at 30 °C, with a low E_a of 8.20 kJ·mol^{-1}. After five cycles reuse, the reaction could keep a conversion rate of about 93% and a reaction rate of 178.71 ml·min^{-1}. According to the kinetic studies, the hydrolysis of AB is of the quasi zero-order reaction for A-15 and the quasi first-order reaction for concentration of AB. XRD, ATR-FTIR and *in-situ* MS results confirmed that the dominant hydrolyzate is boric acid and water participated in this reaction as a hydrogen donor. The proton hydrogen in A-15 could induce equimolar AB hydrolysis in aqueous solution, which means each gram of A-15 can fully react 4.67 mmol AB and release 354.4 ml H_2. A-15 not only provides protons for AB hydrolysis, but also promotes this reaction through the hydrogen bonds interaction with AB (aq). The presence of hydrogen bonds between O in the sulfonic acid group of A-15 and AB (aq) were confirmed through ATR-FTIR. The hydrogen bond between A-15 and AB (aq) promotes the diffusion of AB molecules on the surface of A-15 and reduces the activation barrier of the hydrolysis process by facilitating the cleavage of O—H bond of H_2O, the RDS of AB hydrolysis. The lower activation energy is believed mainly due to the hydrogen release caused by DHB and the RDS promoted by the HB make the overall energy barrier of the reaction reduced. Overall, the performance of A-15 is better than several metal catalysts and liquid acid reported for AB hydrolysis. Meanwhile, as ion-exchange resin, the A-15 also owns the potential to be used in continuous reaction units, and the apparent kinetic data would be helpful for reactor design and modelling. This work is expected to contribute to exploring the mechanism of acid induced AB hydrolysis and developing cost-effective technology routes of hydrogen evolution from AB hydrolysis.

CRediT Authorship Contribution Statement

Yilun Dong: Writing – original draft, Methodology, Data curation, Conceptualization. Kang Xue: Writing – review & editing, Funding acquisition, Data curation, Conceptualization. Zexing He: Methodology, Formal analysis, Data curation. Chongjun Li: Formal analysis, Data curation. Ruijie Gao: Supervision, Conceptualization. Zhenfeng Huang: Supervision, Resources, Conceptualization. Chengxiang Shi: Supervision, Conceptualization. Xiangwen Zhang: Resources, Funding acquisition. Lun Pan: Writing – review & editing, Supervision, Resources, Project administration, Methodology, Conceptualization. Jijun Zou: Supervision, Resources, Project administration, Funding acquisition, Conceptualization.

Declaration of Competing Interest

The authors declare that they have no known competing financial interests or personal relationships that could have appeared to influence the work reported in this paper.

Acknowledgements

The authors appreciate the support from the National Natural Science Foundation of China (22222808, 21978200, 22208330), the Postdoctoral Fellowship Program of CPSF (GZC20241204), the China Postdoctoral Science Foundation-Tianjin Joint Support Program (2023T022TJ) and the Haihe Laboratory of Sustainable Chemical Transformations for financial support.

Supplementary Material

Supplementary data to this article can be found online at https://doi.org/10.1016/j.cjche.2025.02.030.

References

[1] L. Schlapbach, A. Züttel, Hydrogen-storage materials for Mobile applications, *Nature* 414 (6861) (2001) 353–358.
[2] Q.L. Zhu, Q. Xu, Liquid organic and inorganic chemical hydrides for high-capacity hydrogen storage, *Energy Environ. Sci.* 8 (2) (2015) 478–512.
[3] Y.T. Wang, L. Pan, Y.X. Chen, G.Q. Shen, L. Wang, X.W. Zhang, J.J. Zou, Mo-doped Ni-based catalyst for remarkably enhancing catalytic hydrogen evolution of hydrogen-storage materials, *Int. J. Hydrogen Energy* 45 (31) (2020) 15560–15570.
[4] S.Y. Guan, Y.Y. Liu, H.H. Zhang, R.F. Shen, H. Wen, N.X. Kang, J.J. Zhou, B.Z. Liu, Y.P. Fan, J.C. Jiang, B.J. Li, Recent advances and perspectives on supported catalysts for heterogeneous hydrogen production from ammonia borane, *Adv. Sci.* 10 (21) (2023) 2300726.
[5] M. Asim, A. Kurbanov, B. Maryam, M. Ajmal, C.X. Shi, L. Pan, J.J. Zou, Pt@Ni2P/C_3N_4 for charge acceleration to promote hydrogen evolution from ammonia-borane, *Int. J. Hydrogen Energy* 48 (65) (2023) 25423–25437.
[6] Department of Energy, Hydrogen storage [OL], https://www.energy.gov/eere/fuelcells/hydrogen-storage. (Accessed 2 August 2024).
[7] U.B. Demirci, Ammonia borane: an extensively studied, though not yet implemented, hydrogen carrier, *Energies* 13 (12) (2020) 3071.
[8] K.D. Baik, J. Kim, J. Lee, H. Kang, Efficient hydrogen generation of ammonia borane by direct heat supply using a polyimide film heater, *Int. J. Hydrogen Energy* 51 (2024) 167–171.
[9] P. Veeraraghavan Ramachandran, P.D. Gagare, Preparation of ammonia borane in high yield and purity, methanolysis, and regeneration, *Inorg. Chem.* 46 (19) (2007) 7810–7817.
[10] M. Asim, S.G. Zhang, M.H. Ai, B. Maryam, Y.T. Wang, X.D. Li, J. Yang, J.J. Zou, L. Pan, Photohydrolysis of ammonia borane for effective H_2 evolution *via* hot electron-assisted energy Cascade of Au-$WO_{2.72}$/TiO_2, *Ind. Eng. Chem. Res.* 61 (31) (2022) 11429–11435.
[11] X.G. Feng, X.M. Chen, P.T. Qiu, D.P. Wu, E.J.M. Hamilton, J. Zhang, X.N. Chen, Copper oxide hollow spheres: synthesis and catalytic application in hydrolytic dehydrogenation of ammonia borane, *Int. J. Hydrogen Energy* 43 (45) (2018) 20875–20881.
[12] C.H. Liu, Y.C. Wu, C.C. Chou, B.H. Chen, C.L. Hsueh, J.R. Ku, F. Tsau, Hydrogen generated from hydrolysis of ammonia borane using cobalt and ruthenium based catalysts, *Int. J. Hydrogen Energy* 37 (3) (2012) 2950–2959.
[13] M. Chandra, Q. Xu, Room temperature hydrogen generation from aqueous ammonia-borane using noble metal nano-clusters as highly active catalysts, *J. Power Sources* 168 (1) (2007) 135–142.
[14] Y.T. Wang, G.Q. Shen, Y.X. Zhang, L. Pan, X.W. Zhang, J.J. Zou, Visible-light-induced unbalanced charge on NiCoP/TiO_2 sensitized system for rapid H_2 generation from hydrolysis of ammonia borane, *Appl. Catal. B Environ.* 260 (2020) 118183.
[15] H. Wu, Y.J. Cheng, Y.P. Fan, X.M. Lu, L.X. Li, B.Z. Liu, B.J. Li, S.Y. Lu, Metal-catalyzed hydrolysis of ammonia borane: mechanism, catalysts, and challenges, *Int. J. Hydrogen Energy* 45 (55) (2020) 30325–30340.
[16] K. Aranishi, H.L. Jiang, T. Akita, M. Haruta, Q. Xu, One-step synthesis of magnetically recyclable Au/Co/Fe triple-layered core-shell nanoparticles as highly efficient catalysts for the hydrolytic dehydrogenation of ammonia borane, *Nano Res.* 4 (12) (2011) 1233–1241.
[17] Y.W. Yang, Z.H. Lu, X.S. Chen, Cu-based nanocatalysts for hydrogen generation *via* hydrolysis and methanolysis of ammonia borane, *Mater. Technol.* 30 (sup2) (2015) A89–A93.
[18] Q.L. Yao, Z.H. Lu, Y.W. Yang, Y.Z. Chen, X.S. Chen, H.L. Jiang, Facile synthesis of graphene-supported Ni-CeO_x nanocomposites as highly efficient catalysts for hydrolytic dehydrogenation of ammonia borane, *Nano Res.* 11 (8) (2018) 4412–4422.
[19] H.J. Li, Z. Yao, Y.L. Zhu, X.T. Wang, The effect of solvent properties on the hydrogen producing performance of catalytic liquid phase ammonia borane, *Fuel* 325 (2022) 124849.
[20] H.Z. Li, Y.H. Li, J.X. Kang, L. Fan, Q.Y. Yang, S.J. Li, A. Rahman, D.Q. Chen, Reactivity and mechanisms of hydridic hydrogen of B–H in ammonia borane towards acetic acids: the ammonia B-monoacyloxy boranes, *New J. Chem.* 45 (22) (2021) 9904–9911.
[21] Y. Shimizu, A. Miyagi, A.K. Tripathi, T. Nakagawa, Delayed ammonia release of ammonia borane hydrolysis by citric acid, *Int. J. Hydrogen Energy* 82 (2024) 733–739.
[22] M. Chandra, Q. Xu, Dissociation and hydrolysis of ammonia-borane with solid acids and carbon dioxide: an efficient hydrogen generation system, *J. Power Sources* 159 (2) (2006) 855–860.
[23] Ö. Nalan, N. Oktar, N.A. Tapan, Esterification of free fatty acids in waste cooking oils (WCO): role of ion-exchange resins, *Fuel* 87 (10–11) (2008) 1789–1798.
[24] M. Banchero, G. Gozzelino, A simple pseudo-homogeneous reversible kinetic model for the esterification of different fatty acids with methanol in the presence of amberlyst-15, *Energies* 11 (7) (2018) 1843.
[25] P. Barbaro, F. Liguori, Ion exchange resins: catalyst recovery and recycle, *Chem. Rev.* 109 (2) (2009) 515–529.
[26] S.M. You, S.S. Lee, M.H. Ryu, H.M. Song, M.S. Kang, Y.J. Jung, E.C. Song, B.H. Sung, S.J. Park, J.C. Joo, H.T. Kim, H.G. Cha, β-Ketoadipic acid production from poly(ethylene terephthalate) waste *via* chemobiological upcycling, *RSC Adv.* 13 (21) (2023) 14102–14109.
[27] N. Boz, N. Degirmenbasi, D.M. Kalyon, Esterification and transesterification of waste cooking oil over Amberlyst 15 and modified Amberlyst 15 catalysts, *Appl. Catal. B Environ.* 165 (2015) 723–730.
[28] Ö. Derya Öncel, Ş. Tayyibe, Ö. Göksel, M.S. Akkuş, Ö. Gülay, The Hydroloysis of ammonia borane by using Amberlyst-15 supported catalysts for hydrogen generation, *Int. J. Hydrogen Energy* 43 (23) (2018) 10765–10772.
[29] L.Q. Li, C. Tang, X.Y. Cui, Y. Zheng, X.S. Wang, H.L. Xu, S. Zhang, T. Shao, K. Davey, S.Z. Qiao, Efficient nitrogen fixation to ammonia through integration of plasma oxidation with electrocatalytic reduction, *Angew. Chem., Int. Ed.* 60 (25) (2021) 14131–14137.
[30] L. Holub, K. Jeřábek, Influence of partial neutralization on catalytic activity of ion exchange resin, *J. Mol. Catal. Chem.* 231 (1–2) (2005) 21–26.
[31] G.P. Rachiero, U.B. Demirci, P. Miele, Bimetallic RuCo and RuCu catalysts supported on γ-Al_2O_3. A comparative study of their activity in hydrolysis of ammonia-borane, *Int. J. Hydrogen Energy* 36 (12) (2011) 7051–7065.
[32] M. Hu, M. Ming, C.L. Xu, Y. Wang, Y. Zhang, D.J. Gao, J. Bi, G.Y. Fan, Towards high-efficiency hydrogen production through *in situ* formation of well-dispersed rhodium nanoclusters, *ChemSusChem* 11 (18) (2018) 3253–3258.
[33] C.C. Chou, D.J. Lee, B.H. Chen, Hydrogen production from hydrolysis of ammonia borane with limited water supply, *Int. J. Hydrogen Energy* 37 (20) (2012) 15681–15690.
[34] J.F. Shen, L. Yang, K. Hu, W. Luo, G.Z. Cheng, Rh nanoparticles supported on graphene as efficient catalyst for hydrolytic dehydrogenation of amine boranes for chemical hydrogen storage, *Int. J. Hydrogen Energy* 40 (2) (2015) 1062–1070.
[35] S. Akbayrak, Y. Tonbul, Ö. Saim, Ceria supported rhodium nanoparticles: superb catalytic activity in hydrogen generation from the hydrolysis of ammonia borane, *Appl. Catal. B Environ.* 198 (2016) 162–170.
[36] Z. Li, T. He, D. Matsumura, S. Miao, A.N. Wu, L. Liu, G.T. Wu, P. Chen, Atomically dispersed Pt on the surface of Ni particles: synthesis and catalytic function in hydrogen generation from aqueous ammonia–borane, *ACS Catal.* 7 (10) (2017) 6762–6769.
[37] X. Zhao, Y.F. Fu, C. Yao, S.R. Xu, Y. Shen, Q. Ding, D. Wenjing Liu, P. Haibo Zhang, P. Xiaohai Zhou, From boron organic polymers to *in situ* ultrafine nano Pd and Pt: green synthesis and application for high efficiency hydrogen evolution, *ChemCatChem* 11 (9) (2019) 2362–2369.
[38] J.K. Zhang, W.L. Yu, D. Feng, H. Xu, Y. Qin, Porous titania nanotube confined ultrafine platinum catalysts synthesized by atomic layer deposition with enhanced hydrolytic dehydrogenation performance, *Appl. Catal. B Environ.* 312 (2022) 121405.
[39] Y.T. Li, X.L. Zhang, Z.K. Peng, P. Liu, X.C. Zheng, Hierarchical porous g-C_3N_4 coupled ultrafine RuNi alloys as extremely active catalysts for the hydrolytic dehydrogenation of ammonia borane, *ACS Sustainable Chem. Eng.* 8 (22) (2020) 8458–8468.
[40] J.X. Wang, B.Y. Hui, T.Y. Jia, X.Y. Chen, X.F. Yu, L.L. Li, X.H. Zhang, Z.M. Lu, X.J. Yang, PVP-Adjusted crystal surfaces of PtPd nanoparticles for enhancing the catalytic hydrolysis of ammonia borane, *ACS Appl. Nano Mater.* 7 (8) (2024) 9490–9498.
[41] Y.M. Zhu, J.H. Zhang, J. Zhang, B.L. Mao, K.S. Yao, K.X. Song, Nanosized Pd@Ag heterojunction with tunable shapes: morphological modulation for improving plasma-mediated catalytic hydrogen evolution, *Fuel* 361 (2024) 130777.
[42] Q. Xu, M. Chandra, Catalytic activities of non-noble metals for hydrogen generation from aqueous ammonia–borane at room temperature, *J. Power Sources* 163 (1) (2006) 364–370.
[43] J.M. Chen, Z.H. Lu, Y.Q. Wang, X.S. Chen, L. Zhang, Magnetically recyclable Ag/SiO_2–$CoFe_2O_4$ nanocomposite as a highly active and reusable catalyst for H_2 production, *Int. J. Hydrogen Energy* 40 (14) (2015) 4777–4785.

[44] X.N. Chen, J.C. Zhao, S.G. Shore, The roles of dihydrogen bonds in amine borane chemistry, *Acc. Chem. Res.* 46 (11) (2013) 2666–2675.
[45] C.A. Morrison, M.M. Siddick, Dihydrogen bonds in solid BH_3NH_3, *Angew. Chem., Int. Ed.* 43 (36) (2004) 4780–4782.
[46] J.T. Hu, Z.X. Chen, M.X. Li, X.H. Zhou, H.B. Lu, Amine-capped Co nanoparticles for highly efficient dehydrogenation of ammonia borane, *ACS Appl. Mater. Interfaces* 6 (15) (2014) 13191–13200.
[47] S. Swinnen, V.S. Nguyen, M.T. Nguyen, Hydrogen release from ammonia borane and derivatives in the presence of a ruthenium complex incorporating cooperative PNP ligands, *Chem. Phys. Lett.* 513 (4–6) (2011) 195–200.
[48] Q.S. Nian, J.Y. Wang, S. Liu, T.J. Sun, S.B. Zheng, Y. Zhang, Z.L. Tao, J. Chen, Aqueous batteries operated at −50 °C, *Angew. Chem., Int. Ed.* 58 (47) (2019) 16994–16999.
[49] X.D. Chen, X.L. Luo, X.F. Zhang, H.Z. Wang, Y.C. Li, L.F. Ye, J.H. Zheng, H. Li, Regulation of electronic structures of the urchin-like NiCoP/CoP nanocatalysts for fast hydrogen evolution, *Chemistry* 30 (23) (2024) e202304266.
[50] Q. Wang, F.Y. Fu, S. Yang, M. Martinez Moro, M. de los Angeles Ramirez, S. Moya, L. Salmon, J. Ruiz, D. Astruc, Dramatic synergy in CoPt nanocatalysts stabilized by "click" dendrimers for evolution of hydrogen from hydrolysis of ammonia borane, *ACS Catal.* 9 (2) (2019) 1110–1119.
[51] K. Wang, Y. Jing, X.R. Yin, X.M. Chen, X.N. Chen, Synthesis of aminodiborane through the reaction of ammonia borane with acids, *Inorg. Chem.* 63 (46) (2024) 22118–22123.
[52] F.H. Stephens, R. Tom Baker, M.H. Matus, D.J. Grant, D.A. Dixon, Acid initiation of ammonia-borane dehydrogenation for hydrogen storage, *Angew. Chem. Int. Ed.* 46 (5) (2007) 746–749.
[53] I.V. Fedorova, L.P. Safonova, Comparisons of NH…O and OH…O hydrogen bonds in various ethanolammonium-based protic ionic liquids, *Struct. Chem.* 32 (5) (2021) 2061–2073.
[54] L.M. Wang, Clusters of hydrated methane sulfonic acid $CH_3SO_3H.(H_2O)_n$ (n = 1–5): a theoretical study, *J. Phys. Chem. A* 111 (18) (2007) 3642–3651.
[55] W.Y. Chen, D.L. Li, Z.J. Wang, G. Qian, Z.J. Sui, X.Z. Duan, X.G. Zhou, I. Yeboah, D. Chen, Reaction mechanism and kinetics for hydrolytic dehydrogenation of ammonia borane on a Pt/CNT catalyst, *AIChEJ.* 63 (1) (2017) 60–65.
[56] P. Hodge, Polymer-supported organic reactions: what takes place in the beads? *Chem. Soc. Rev.* 26 (6) (1997) 417.